*The Company of* **Biologists**

## RESEARCH ARTICLE

# Cardiomyocyte ploidy is dynamic during postnatal development and varies across genetic backgrounds

Samantha K. Swift[1], Alexandra L. Purdy[1], Mary E. Kolell[1], Kaitlyn G. Andresen[1], Caitlin Lahue[2], Tyler Buddell[1,3], Kaelin A. Akins[1], Christoph D. Rau[2], Caitlin C. O'Meara[3,4] and Michaela Patterson[1,3,*]

## ABSTRACT

Somatic polyploidization, an adaptation by which cells increase their DNA content to support growth, is observed in many cell types, including cardiomyocytes. Although polyploidization is believed to be beneficial, progression to a polyploid state is often accompanied by loss of proliferative capacity. Recent work suggests that genetics heavily influence cardiomyocyte ploidy. However, the developmental course by which cardiomyocytes reach their final ploidy state has only been investigated in select backgrounds. Here, we assessed cardiomyocyte number, cell cycle activity, and ploidy dynamics across two divergent mouse strains: C57BL/6J and A/J. Both strains are born and reach adulthood with comparable numbers of cardiomyocytes; however, the end composition of ploidy classes and developmental progression to reach the final state differ substantially. We expand on previous findings that identified *Tnni3k* as a mediator of cardiomyocyte ploidy and uncover a role for *Runx1* in ploidy dynamics and cardiomyocyte cell division, in both developmental and injury contexts. These data provide novel insights into the developmental path to cardiomyocyte polyploidization and challenge the paradigm that hypertrophy is the sole mechanism for growth in the postnatal heart.

KEY WORDS: Cardiomyocyte, Somatic polyploidy, Endomitosis, Proliferation, Regeneration

## INTRODUCTION

Somatic polyploidization, a cellular process resulting in the retention of multiple copies of the archetypical diploid genome, is a key component of development and organogenesis for many mammalian tissues, including the heart. Cardiomyocytes transition to a polyploid state beginning around birth, with the exact timing being species specific (Gan et al., 2020; Patterson and Swift, 2019). Polyploidization largely coincides with the shift from hyperplastic to hypertrophic growth of the myocardium (Soonpaa et al., 1996). Although the exact function of somatic polyploidy in cardiomyocytes is still not fully understood, it has been implicated in energy preservation during rapid postnatal growth, maintenance of intercalated discs and the pseudosyncitium, establishment of greater force-generating muscle units, and differentiation to a post-mitotic state (Orr-Weaver, 2015; Patterson and Swift, 2019). Insights into the developmental progression to cardiomyocyte polyploidy would improve our understanding of specific aspects of myocardial biology, including total cardiomyocyte number, cell cycle potential in naïve and disease contexts, and capacity for myocardial regeneration.

Cardiomyocyte polyploidy arises via an alternative cell cycle known as endomitosis, in which cells replicate their genome without completing mitosis. Insights from mouse studies suggest that cardiomyocyte polyploidization is tightly linked to cell cycle exit. For example, in the mouse, cardiomyocyte completion of cell division rapidly declines within the first 1-2 days of birth and DNA synthesis during the first postnatal week largely contributes to cardiomyocyte polyploidization. Subsequently, additional DNA synthesis ceases around postnatal day (P) 10, at which point both the ploidy state of individual cardiomyocytes and the final number of cardiomyocytes are thought to be largely determined and constant (Alkass et al., 2015; Soonpaa et al., 1996, 2015; Walsh et al., 2010). The timeline of cell cycle exit is further supported by the loss of cardiac regenerative capacity after P7 in mice (Porrello et al., 2011). Strikingly, ploidy in other cell types, such as hepatocytes, is not believed to be static as has been proposed in cardiomyocytes, but is instead a fluid and dynamic state (Duncan, 2013).

Cardiomyocytes display diverse ploidy states. A single round of endomitosis results in cells with twice as much DNA (i.e. 4N), and a second round of endomitosis would produce 8N cells. Another layer of complexity arises from the stage at which a cardiomyocyte exits the cell cycle. Cardiomyocytes can exit the endomitotic cell cycle just prior to karyokinesis resulting in single-nucleus, polyploid cells ($1\times4N$, $1\times8N$, etc.). Conversely, cardiomyocytes can successfully complete karyokinesis but fail to complete cytokinesis resulting in multinucleated cells with diploid nuclei ($2\times2N$, $4\times2N$, etc.). In some cases, a combination of the two exit points ensues ($2\times4N$, or trinucleated $1\times4N;2\times2N$). Together, these cell fate decisions contribute to a final composition of diverse ploidy classes, which display both inter- and intraspecies variation. For example, human cardiomyocytes are predominantly mononuclear and polyploid (Mollova et al., 2013), whereas murine cardiomyocytes are predominantly binucleated (Soonpaa et al., 1996), and porcine cardiomyocytes can have upwards of 16 diploid nuclei (Velayutham et al., 2020). An interesting question that has arisen from the field is whether the various ploidy classes bestow distinct attributes to the myocardium. Recent literature suggests that having a higher proportion of mononuclear diploid cardiomyocytes (MNDCMs, $1\times2N$) is associated with greater regenerative competence, and polyploidy in cardiomyocytes impairs the proliferative response (Gonzalez-Rosa et al., 2018; Han et al., 2020; Hirose et al., 2019; Patterson et al., 2017). Beyond regeneration, the roles that distinct

[1]Medical College of Wisconsin, Department of Cell Biology, Neurobiology, and Anatomy, Milwaukee, WI 53226, USA. [2]University of North Carolina School of Medicine, Department of Genetics, Chapel Hill, NC 27599, USA. [3]Medical College of Wisconsin, Cardiovascular Center, Milwaukee, WI 53226, USA. [4]Medical College of Wisconsin, Department of Physiology, Milwaukee, WI 53226, USA.

*Author for correspondence (mpatterson@mcw.edu)

S.K.S., 0000-0002-5618-7578; A.L.P., 0000-0003-1632-5523; T.B., 0000-0002-2591-1375; K.A.A., 0000-0002-1205-7210; C.D.R., 0000-0002-0782-207X; C.C.O., 0000-0002-9212-0821; M.P., 0000-0002-3805-4181

DEVELOPMENT

1

ploidy classes play in cardiac homeostasis and pathophysiology remain largely unexplored.

Much of our understanding surrounding the timing and progression of polyploidy stems from work on mice and is limited to only a few strains. We recently determined that ploidy class ratios vary dramatically across inbred mouse strains, whereby some strains have a higher proportion of MNDCMs, and other strains display higher proportions of cardiomyocytes with ≥8N DNA content (Patterson et al., 2017). These findings suggest that genetics influence cardiomyocyte ploidy composition and raise the concern that our insights into polyploid progression and cardiomyocyte cell cycle dynamics may be hampered by only examining the process in select strains. We initiated the experiments described here on the basis of the hypothesis that two strains of mice with divergent ploidy composition in adulthood arise at their terminal states via distinct approaches.

## RESULTS
### Polyploidization of C57BL/6J and A/J cardiomyocytes follow distinct developmental programs

We sought to characterize the progression of cardiomyocyte polyploidy from the early postnatal period through adulthood across two genetically and phenotypically divergent, inbred mouse strains: A/J and C57BL/6J. These strains were selected based on the demonstration by Patterson et al. (2017) that A/J had fivefold higher MNDCM content than C57BL/6J at 6 weeks of age. First, we established the total number of cardiomyocytes in both C57BL/6J and A/J ventricles at multiple time points, ranging from P1 to 6 weeks of age (Fig. 1A; see Table S1 for detailed statistics). Cardiomyocytes were counted using a hemocytometer and distinguished from non-cardiomyocytes by morphology and size. We found C57BL/6J mice had a significant increase in the number of cardiomyocytes from P1 to P7 ($P<0.001$), after which total cardiomyocyte number displayed minimal expansion ($P=0.077$ P7 to 6 weeks of age). This result is consistent with previous literature for C57BL/6N, C57BL/6J and DBA/2J mice (Alkass et al., 2015; Soonpaa et al., 2015) and suggests that some residual completion of the canonical mitotic cell cycle takes place after birth. Conversely, A/J ventricles demonstrated a slower, although still significant, initial increase in cardiomyocyte numbers in the week immediately following birth ($P=0.041$). Unlike C57BL/6J mice, a second significant increase in cardiomyocyte numbers occurred from P21 to 6 weeks in A/J mice ($P=0.030$; Fig. 1A).

Alongside our assessment of total cardiomyocyte number, we examined the dynamics of polyploidization across the two strains from P7 to 6 weeks of age. In single-cell suspensions generated from Langendorff-digested ventricles, we quantified various ploidy classes, including MNDCMs (2N – 1×2N), tetraploid cardiomyocytes (4N – 1×4N and 2×2N), octoploid cardiomyocytes (8N – 1×8N; 2×4N; trinucleated – 1×4N and 2×2N; and 4×2N), and a rare 16N cardiomyocyte (Fig. 1B,C). This analysis revealed that C57BL/6J mice display a substantial increase in cardiomyocyte polyploidization from P7 to P14, at which point only 2.5% of cardiomyocytes remained mononuclear and diploid (Fig. 1C,D). The vast majority of cardiomyocytes were 4N by P7 and this ploidy class remained the majority at 6 weeks. Octoploid cardiomyocytes most strikingly increased in number during the second postnatal week (from P7 to P14), suggesting that a second round of endomitosis takes place during this time. Very little change in ploidy states occurred after P14 other than a slight further expansion of the 8N population from P14 to 6 weeks ($P=0.037$) (Fig. 1C; see Table S2 for detailed statistics). A/J cardiomyocyte

ploidy increased until P21 when the frequency of a residual MNDCM population reached its lowest point and the frequency of the 8N population its maximum (Fig. 1C,D). Surprisingly, between P21 and 6 weeks of age the MNDCM population nearly doubled in size from 3.9% at P21 to 7.6% at 6 weeks ($P=0.006$), a phenomenon that was not observed in C57BL/6J (Fig. 1D). To narrow the window of when this expansion occurred, we added a 4-week-old collection time point for A/J mice, demonstrating that the increase of the MNDCM population largely took place during the fourth postnatal week of life. This expansion coincided with the second wave of increased cardiomyocyte numbers unique to A/J mice (Fig. 1A). These observed cellular differences between strains did not significantly impact body weight (Fig. S1A), heart weight (Fig. S1B), or heart-weight-to-body-weight ratios (Fig. S1C) at the time points assessed.

To identify an explanation for the robust expansion of MNDCMs after P21 in A/J mice, we assessed DNA synthesis by intraperitoneal (i.p.) injections of 5-ethynyl-2′-deoxyuridine (EdU) at select time points throughout postnatal development and evaluation by in situ immunofluorescence (Fig. 1E) 1 day after the final injection (Fig. 1F). Both C57BL/6J and A/J hearts displayed the highest level of DNA synthesis at P4. DNA synthesis reached near negligible levels in both strains by the third postnatal week, consistent with previous reports (Soonpaa et al., 1996, 2015). At P7 and P10, A/J mice showed significantly reduced numbers of EdU-positive cardiomyocytes. This aligned with our observation of a slower increase in total cardiomyocyte number compared with C57BL/6Js (Fig. 1A) and slower conversion to polyploid states (Fig. 1C,D). From P21 onward, very few EdU-positive cardiomyocytes were identified in either strain (Fig. 1F). Furthermore, we detected no increase in DNA synthesis in A/J compared with C57BL/6J during the 3- to 4-week time point, suggesting that the robust expansion of A/J cardiomyocytes observed between P21 and 4 weeks could not be explained by traditional mitotic expansion of the MNDCM population. Concerned that we might have missed a pertinent population of cycling cardiomyocytes by two-chamber histology, we again quantified EdU incorporation in both four-chamber views and single-cell suspensions following Langendorff digestion of whole ventricles and found equally low levels of EdU-positive cardiomyocytes compared with the original two-chamber quantifications (S.K.S., unpublished observations).

### A/J cardiomyocytes display delayed cell division following weaning

To investigate the expansion of MNDCM frequency in A/J mice between P21 and 6 weeks of age in the absence of new DNA synthesis, we quantified the completion of cell division by a single-cell suspension method in both A/J and C57BL/6J mice (Fig. 2A-C). Briefly, if a cardiomyocyte labeled with EdU is both mononuclear and diploid it is interpreted to have completed cell division (Fig. 2A; Auchampach et al., 2022). We used this logic to see whether we could detect 1×2N EdU-positive cardiomyocytes at a time point after the observed MNDCM expansion at 6 weeks, which were not present at P21. To achieve this, we labeled cardiomyocytes with daily 10 mg/kg injections of EdU from P14-20. Following EdU administration, we analyzed nucleation and ploidy of EdU-positive cardiomyocytes at two time points, P21 or 6 weeks of age, by single-cell suspension methods (Fig. 2B,C). With this EdU regimen, P21 A/J ventricles displayed a slight reduction in the frequency of EdU-positive cardiomyocytes compared with C57BL/6J ventricles (Fig. 2D). This decreased EdU incorporation was not
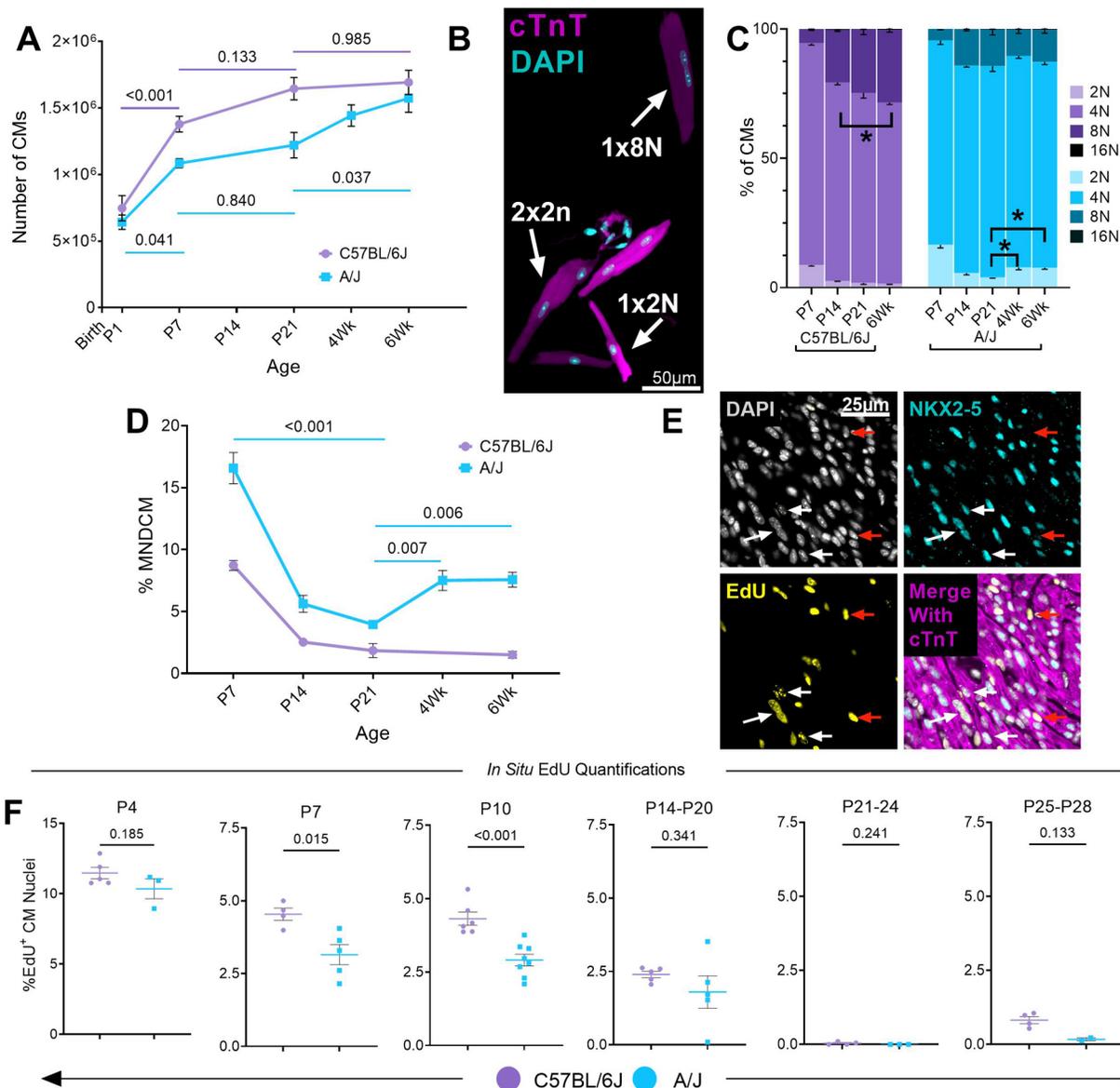
2

**Fig. 1. Developmental progression of polyploidy across genetically divergent mouse strains.** (A) Number of cardiomyocytes counted by hemocytometer after Langendorff dissociation over multiple time points from P1 to 6 weeks of age in C57BL/6J (purple) and A/J mice (blue) (*n*=6-14). Complete breakdown of data and statistical comparisons can be found in Table S1. (B) Single-cell ventricular suspension stained for cardiac troponin T (cTnT) (magenta) and DAPI (cyan). Identified cardiomyocyte ploidy classes are indicated. (C) Quantification of 2N (1×2N), 4N (sum of 1×4N and 2×2N populations), 8N [sum of 1×8N, 2×4N, tri (1×4N+2×2N) and 4×2N populations] and 16N [sum of 1×16N, 2×8N, tri (1×8N+2×4N) and 4×4N populations] ploidy classes at multiple time points from P7 to 6 weeks in C57BL/6J and A/J mice (*n*=3-9). *P<0.05 for select comparisons; complete statistical comparisons can be found in Table S2. (D) Percentage MNDCMs extracted from the data shown in C (*n*=3-9). (E) Representative images of cardiomyocyte DNA synthesis measured *in situ* with DAPI (gray), NKX2-5 (cyan), EdU (yellow) and cTnT (magenta). White arrows indicate EdU/NKX2-5 double-positive cardiomyocyte nuclei, red arrows indicate EdU-positive NKX2-5-negative non-cardiomyocyte nuclei. (F) Quantification of the percentage of EdU/NKX2-5 double-positive nuclei as a percentage of total NKX2-5-positive cardiomyocyte nuclei in the left ventricle in both strains across multiple time points. Time points above each graph indicate the time of the EdU injection. Tissue was collected 24 h after last injection. *P*-values in most panels calculated by two-tailed, unpaired Student's *t*-test, with the exception of P14-P20, which was calculated by a two-tailed, unpaired Welch's *t*-test. Complete breakdown of *n* and litter contributions can be found for all experiments in Table S3. Data are mean±s.e.m. CM, cardiomyocyte.

detected by *in situ* quantification methods with a similar injection strategy, but is consistent with observations at other time points assessed *in situ* (i.e. P7 and P10; Fig. 1F). In line with our previous data, and the current literature, C57BL/6J mice had few or no EdU-positive MNDCMs at either the P21 or the 6-week collection time point (Fig. 2E), suggesting that EdU injections in the third postnatal week do not contribute to cell division. Instead, the vast majority of C57BL/6J cardiomyocytes undergoing DNA synthesis during the

third postnatal week were becoming 8N (Fig. 2F), likely arising from a 4N cell undergoing a second round of endomitosis. In contrast, EdU-positive MNDCMs could be found at both P21 and 6 weeks of age in A/J mice, suggesting that some completion of cell division is still taking place. Most surprisingly, despite identical EdU injection regimens and random segregation of littermates across time points to avoid batch effects, we quantified a more than twofold increase in EdU-positive MNDCMs at the 6-week time
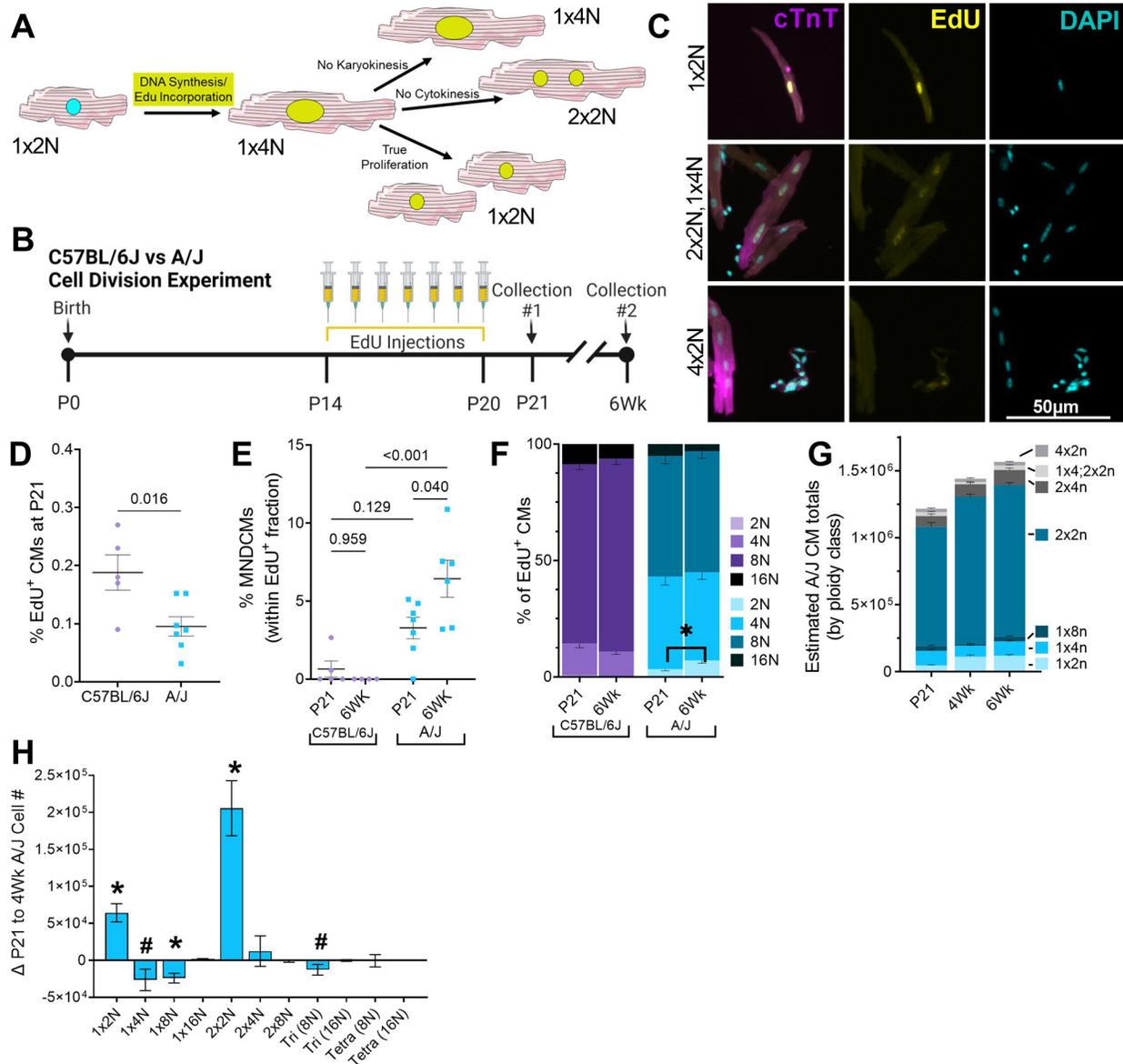
**Fig. 2. A/J cardiomyocytes undergo cell division after P21 resulting in expansion of the MNDCM population.** (A) Schematic depicting possible outcomes after EdU labeling. EdU-positive cardiomyocytes can only become mononuclear and diploid if the cell cycle was successfully completed. (B) Timeline of EdU injections and cell collection time points. (C) Representative images of single-cell ventricular suspensions stained for cTnT (magenta), EdU (yellow) and DAPI (cyan). Tri- and tetranucleated cardiomyocytes are used to normalize DAPI fluorescence intensity. Top: EdU-positive MNDCM (1×2N); middle: EdU-positive trinucleated cardiomyocyte (2×2N; 1×4N); and bottom: EdU-negative tetranucleated cardiomyocyte (4×2N). (D) Quantification of total EdU-positive cardiomyocytes following EdU administration as outlined in B represented as a percentage of total cardiomyocytes. Assessed at P21 collection time point. $P$-value calculated by unpaired, two-tailed Student's $t$-test. (E) Quantification of EdU-positive MNDCMs as a percentage of total EdU-positive cardiomyocytes in both A/J and C57BL/6J at P21 and 6 weeks of age. $P$-values calculated by a two-way ANOVA with Tukey HSD posthoc analysis. (F) Quantification of EdU-positive cardiomyocytes broken down into total DNA content (i.e. 2N, 4N, 8N or 16N). $P$-values calculated by a MANOVA with Tukey HSD posthoc analysis. (G) Estimated total number of cardiomyocytes in A/J for each ploidy class. Calculations were determined by multiplying the total number of cardiomyocytes (Fig. 1A) by the percentage of each ploidy class (Fig. 1C) at P21, 4 weeks and 6 weeks. (H) Difference in cardiomyocyte cell number from P21 to 4 weeks by ploidy class. *$P<0.05$; #$P\leq0.1$. $P$-values calculated from parent graph in G with MANOVA and posthoc Tukey HSD. Complete breakdown of $n$ and litter contributions can be found for all experiments in Table S3. Data are mean±s.e.m. CM, cardiomyocyte.

point compared with P21 in A/J hearts (~2.5% to ~6%, $P=0.04$; Fig. 2E). These data imply that a subset of cardiomyocytes that underwent DNA synthesis during the third postnatal week does not complete cell division until after P21.

To refine which weeks of postnatal development were contributing to cardiomyocyte cell cycle completion in A/J mice, we conducted two additional single-cell suspension division experiments in A/J alone, labeling with EdU during earlier

developmental time points either at the first (Fig. S2A) or the second (Fig. S2D) postnatal weeks, and assessing for cell division at P21 and 4 weeks. When labeling in the first week at P4 and P5, a similar phenotype was observed as with the third postnatal week labeling strategy: EdU-positive MNDCMs were more frequently identified at 4 weeks (3.03%) compared with P21 (1.18%) (Fig. S2B; $P=0.001$). However, there were nominal numbers (<1%) of EdU-positive MNDCMs identified at P21 and 4 weeks

when labeling in the second postnatal week (Fig. S2E), indicating the DNA synthesis occurring during the second postnatal week primarily contributes to polyploidization of cardiomyocytes. More specifically, 80% of cardiomyocytes undergoing DNA synthesis in this second postnatal week were becoming ≥8N (Fig. S2F). This was a greater percentage of ≥8N cardiomyocytes than was seen with injection regimens at any other time point (Fig. 2F, Fig. S2C).

Upon confirmation of delayed cell division in A/J mice, we attempted to elucidate whether any ploidy classes were reciprocally declining in size to account for the expansion of the MNDCM population. To derive an estimate of the total number of cardiomyocytes in each ploidy class at each time point, the ploidy class percentages at P21, 4 weeks and 6 weeks were multiplied by the total cardiomyocyte numbers at each respective time point (Fig. 2G). With this calculation, we could again confirm that the 1×2N population had expanded in total number from P21 to 4 weeks of age by a mean of ~64,000 cardiomyocytes (Fig. 2G,H; $P<0.0002$). We also detected a significant increase in the 2×2N population. As for populations that were decreasing over this same period, only the 1×8N population reached statistical significance decreasing by ~24,000 cells between P21 and 4 weeks (Fig. 2H; $P=0.002$); however, other populations also decreased with less confidence, including the 1×4N (~26,000; $P=0.10$) and trinucleated, 1×4N and 2×2N, populations (~12,000; $P=0.08$) (Fig. 2H). These results suggest that while the 1×2N population is expanding in total number as a result of delayed cell cycle completion, the 1×8N cardiomyocyte population, and possibly additional polyploid populations, are reciprocally declining in total number.

Past analysis from just one or two mouse strains, including C57BL/6-related strains, has suggested that cardiomyocyte ploidy is largely static after about P14 (Alkass et al., 2015; Soonpaa et al., 1996, 2015; Walsh et al., 2010). Our detailed analysis presented here suggests a much more dynamic process in A/J hearts, whereby a subset of cardiomyocytes, which undergo DNA synthesis in the first postnatal week and again in the third postnatal week, complete cell division sometime after weaning.

### *Tnni3k* hypomorphism is partially responsible for ploidy dynamics

We next began to explore possible mechanisms for this unique and dynamic ploidy phenotype observed in A/J mice. A/J mice harbor a naturally occurring hypomorphic mutation in the gene *Tnni3k* (Wheeler et al., 2009), whereas C57BL/6J carry the 'wild-type' variant. Utilizing an engineered knockout allele of *Tnni3k* maintained on a C57BL/6J inbred background, Patterson et al. (2017) previously established that genetic ablation of *Tnni3k* contributes to MNDCM frequency. Specifically, *Tnni3k* knockout mice display a MNDCM frequency of 5.3% in early adulthood compared with just 1.5% in controls (Patterson et al., 2017). Additional loss-of-function alleles of *Tnni3k* have yielded similar results (Gan et al., 2021, 2019). Knowing that *Tnni3k* partially contributes to the end-state frequency of MNDCMs, we hypothesized that *Tnni3k* also plays a role in the ploidy dynamics observed after P21 in A/J mice. To test this, we examined ploidy composition (Fig. 3A) and total cardiomyocyte numbers (Fig. 3B) in *Tnni3k* global knockout mice ($Tnni3k^{-/-}$) compared with wild-type littermates ($Tnni3k^{+/+}$) maintained on a C57BL/6J background. At P21, MNDCM frequency was not different across genotypes, both fell below 2% (Fig. 3A). From 3-6 weeks of age, $Tnni3k^{+/+}$ MNDCM numbers stayed constant at around 1-1.5%.

However, MNDCM frequency in $Tnni3k^{-/-}$ mice gradually increased over this same time course ($P=0.02$). At early adulthood, *Tnni3k* knockout mice had three times more MNDCMs than wild-type littermates ($P=0.009$), but this was still only one-third the number of MNDCMs typically observed in A/J mice, consistent with previous reports (Patterson et al., 2017). Total cardiomyocyte number did not increase between the P21 and 6-week time points in knockout animals, nor did it differ across genotypes (Fig. 3B). When we repeated the cell division experiment shown in Fig. 2B (daily EdU injections from P14-P20) in these animals, there were fewer total EdU-positive cardiomyocytes in $Tnni3k^{-/-}$ mice (Fig. 3C; $P=0.0006$), consistent with recent literature (Reuter et al., 2022) and with what we observed in A/J mice by this same method (Fig. 2D). Strikingly, at 6 weeks, we saw significantly more EdU-positive MNDCMs in $Tnni3k^{-/-}$ compared with $Tnni3k^{+/+}$ mice (Fig. 3D; $P=0.012$). However, comparison of $Tnni3k^{-/-}$ 6-week preparations with those at P21 revealed only a trending increase in EdU-positive MNDCMs (Fig. 3D). Furthermore, the frequency of EdU-positive MNDCMs were even more rare than observed in A/J with this same injection regimen (Fig. 2E). Taken together, these data suggest that *Tnni3k* hypomorphism is only partially responsible for the ploidy phenotypes observed in A/J mice.

### A genetic locus, including *Runx1*, associates with MNDCM frequency

To identify additional genetic contributors to ploidy dynamics observed in A/J mice, we returned to a genome-wide association study (GWAS) published by Patterson et al. (2017), which mapped frequency of mononuclear cardiomyocytes across the Hybrid Mouse Diversity Panel (HMDP). With any genetic resource, including the HMDP, relevant genetic loci may be masked by complex gene–gene interactions, including additive, suppressive or epistatic relationships. Within the HMDP there are four panels of recombinant inbred (RI) strains: BXD (C57BL/6J×DBA/2J), AXB/BXA (A/J×C57BL/6J, and vice versa), BXH (C57BL/6J×C3H/J), and CXB (Balb/cJ×C57BL/6J); inclusion of any one of the RI panels could suppress or wash out a relevant locus. With this logic, we re-ran the original phenotypic data, frequency of mononuclear cardiomyocytes across 120 strains, but excluded the BXD panel (44 strains), and a locus on chromosome (Chr) 16 rose in significance (Fig. 4A versus 4B; Patterson et al., 2017). With the BXD panel removed, the AXB/BXA RI panel makes up 35% of the remaining data (27 AXB/BXA strains of 76 total remaining strains after BXDs have been removed); thus, it is a major contributor to the statistical significance. Interestingly, when the AXB/BXA panel is instead removed from the phenotype data, the locus is completely lost (Fig. 4C). Taken together, these observations indicate that the Chr16 locus associated with the frequency of mononuclear cardiomyocytes is dependent on polymorphisms between A/J and C57BL/6J.

Based on criteria set by Wang et al. (2016) for determining locus range, the identified Chr16 locus spans approximately 4.2 Mbps: 89,459,997 (*Tiam*) to 93,665,575 (*Dop1b*). In another study using the HMDP, we used reduced representational bisulfite sequencing to identify changes to CpG methylation sites that affect cardiac phenotypes. Using the same BXD-removed data, which identify the genomic locus, we performed an epigenome-wide association study (EWAS) and identified a locus-wide significant association ($P=3.9E^{-04}$) between the methylation status of a CpG within the locus and the percentage of mononuclear cardiomyocytes. Leveraging the significantly smaller block sizes of EWAS loci
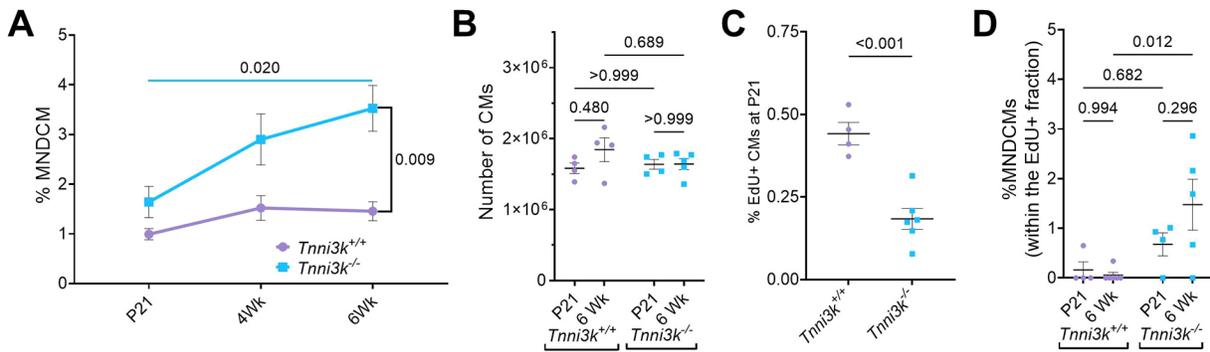
**Fig. 3.** *Tnni3k* **ablation in C57BL/6J partially phenocopies A/J ploidy dynamics.** (A) Percentage of MNDCMs over time in *Tnni3k⁻/⁻* versus *Tnni3k⁺/⁺* (maintained on a C57BL/6J background). *P*-value calculated by two-way ANOVA with Tukey HSD posthoc analysis. (B) Number of cardiomyocytes counted by hemocytometer after Langendorff dissociation at P21 and 6 weeks of age (*n*=4-5). *P*-values calculated by two-way ANOVA with Tukey HSD posthoc analysis. (C) Percentage of EdU-positive cardiomyocytes at P21 following P14-P20 daily EdU injections. *P*-value calculated by unpaired, two-tailed Student's *t*-test. (D) Quantification of EdU-positive MNDCMs represented as a percentage of total EdU-positive cardiomyocytes in *Tnni3k⁻/⁻* and *Tnni3k⁺/⁺* at P21 and 6 weeks. *P*-values calculated by two-way ANOVA with Tukey HSD posthoc analysis. Complete breakdown of *n* and litter contributions can be found for all experiments in Table S3. Data are mean±s.e.m. CM, cardiomyocyte.

(Orozco et al., 2015), we were able to narrow down the Chr16 locus further to approximately 92,763,000-93,665,500. Within this refined locus are only six protein-coding genes: *Runx1*, *1810053B23Rik*, *Setd4*, *Cbr1*, *Cbr3* and *Dop1b*. Of these six genes, we identified *Runx1* as an interesting candidate as it has been used as a marker of cardiomyocyte regression to a less differentiated state prior to cell cycle re-entry (D'Uva et al., 2015; Kubin et al., 2011). With this in mind, we first investigated whether Runx1-positive cardiomyocytes were more prevalent in A/J than in C57BL/6J hearts at P21, just preceding expansion of the MNDCM population in A/J mice. Given that DNA synthesis was not different across strains at this time point, we instead combined RUNX1 antibody stain with a more general cell cycle marker, Ki67 (Fig. 4D). A/J ventricles displayed almost threefold more RUNX1-positive cardiomyocytes than did C57BL/6J ventricles (Fig. 4E). Additionally, RUNX1-positive cardiomyocytes were frequently double positive for Ki67 (Fig. 4F). Very few RUNX1-positive, Ki67-negative cardiomyocytes were found in either strain.

### *Runx1* overexpression is sufficient to expand the MNDCM population and induce cardiomyocyte proliferation in C57BL/6J

To test directly the ability of *Runx1* to induce A/J-like phenotypes in C57BL/6J mice, we utilized a conditional overexpression allele whereby *Runx1* cDNA preceded by a *LoxP-STOP-LoxP* cassette was inserted into the ubiquitous *Rosa26* locus [*Gt(Rosa)26*ᵗᵐ¹⁽ᴿᵁᴺˣ¹⁾ᴹᵅ, referred to throughout as Runx1ᴼᴱ] (Qi et al., 2017; Yzaguirre et al., 2018). When crossed to the *Myh6-MerCreMer* driver (JAX Stock 011038), these mice overexpress *Runx1* only in cardiomyocytes following tamoxifen induction. Both alleles have been backcrossed and maintained on a C57BL/6J background in our laboratory. Mice with a single copy of the *Runx1* transgene were crossed to mice with two copies of the *Cre* transgene, resulting in litters with either *Myh6-MerCreMer⁺/⁻* only (Ctrl) or *Myh6-MerCreMer⁺/⁻; Rosa26*ᵗᵐ¹⁽ᴿᵁᴺˣ¹⁾ᴹᵅ (Runx1ᴼᴱ). All animals received tamoxifen, which was administered with two subcutaneous injections at P0 and P1 (Fig. 4G). With this injection regimen, we observed that most cardiomyocytes expressed RUNX1 (Fig. S3A). Animals were also injected with EdU at P4 and P5 and hearts were collected at 4 weeks of age as a single-cell suspension for nucleation and ploidy analysis (similar to Fig. S2A). First,

considering all cardiomyocytes regardless of EdU status, Runx1ᴼᴱ mice displayed twice as many MNDCMs compared with Ctrl littermates (*P*=0.015; Fig. 4H). There was no measurable change in the number of EdU-positive cardiomyocytes with this injection regimen (Fig. S3B); however, we did observe a significant increase in the number of EdU-positive MNDCMs, suggesting they had completed cell division (*P*=0.023; Fig. 4I). Furthermore, this resulted in an increase in total cardiomyocyte number, from 1.74 million in Ctrl hearts to 2.10 million in Runx1ᴼᴱ hearts (*P*=0.017; Fig. 4J). Taken together, these data indicate that *Runx1* is sufficient to induce cardiomyocyte proliferation in C57BL/6J mice.

### *Runx1* overexpression at the time of myocardial infarction increases cell cycle activation and completion

Given the robust effect on cardiomyocyte proliferation during postnatal development, we sought to evaluate whether *Runx1* can similarly induce cardiomyocyte proliferation and myocardial regeneration in an injury context. Here, we simulated myocardial infarction (MI) by permanent ligation of the left anterior descending (LAD) artery on the 8- to 10-week-old Runx1ᴼᴱ mice compared with littermate Ctrls. *Runx1* overexpression in cardiomyocytes was induced with tamoxifen injections on day 0 and day 1 post-MI. Cardiac function was evaluated by echocardiography 3 days prior to injury, and 3, 14 and 28 days post-injury (dpi). Cell cycle activity occurring shortly after injury was measured with five single EdU injections from 6 to 10 dpi and mice were collected at 28 dpi (Fig. 5A). Runx1ᴼᴱ mice displayed transient enhanced fractional shortening assessed by M-mode at the mid-papillary height compared with Ctrl mice at 14 dpi (*P*=0.029), but this difference was not observed at 28 dpi (Fig. 5B). B-mode assessment of ejection fraction instead suggested no difference across genotypes (Fig. S4). Masson Trichrome stains (Fig. 5C) were performed on histological sections collected at 28 dpi and on histological sections from an independent cohort collected at 14 dpi. Analysis of scar size at 14 dpi confirmed smaller scars at 14 dpi (Fig. 5D; *P*=0.033), but not at 28 dpi (Fig. 5E), in line with the transient enhancement of fractional shortening. Impressively, 28 dpi histological analysis for cardiomyocyte cell cycle activation in the infarct border zone (Fig. 5F) identified an almost fourfold increase in EdU-positive NKX2-5-positive cardiomyocytes (Fig. 5G; *P*=0.002). This analysis most likely identifies cardiomyocytes that were cycling
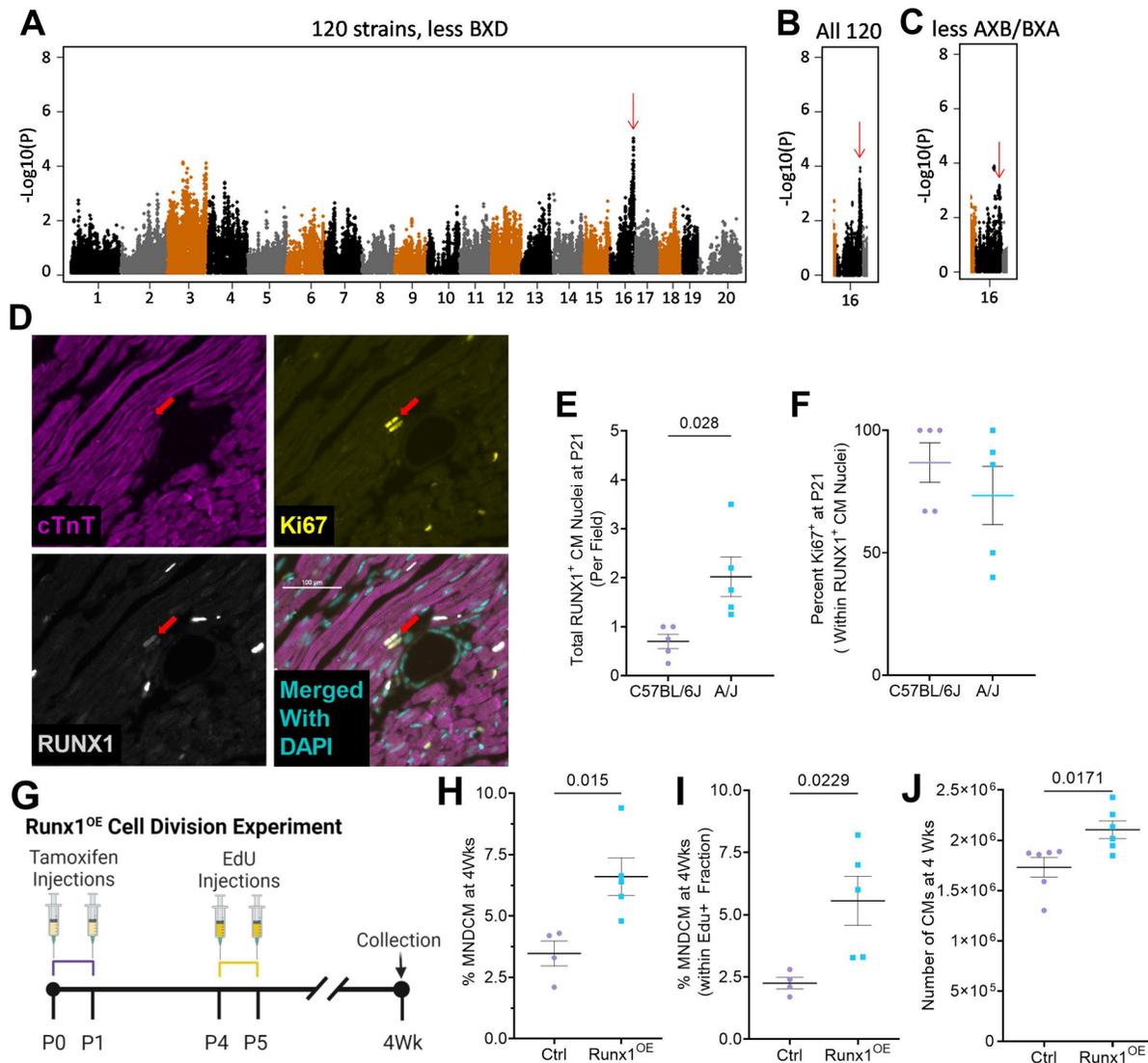
**Fig. 4. *Runx1* overexpression in C57BL/6J is sufficient to induce A/J-like ploidy phenotypes.** (A) Manhattan plot for genome association utilizing phenotypic data collected by Patterson et al. (2017) after removing the BXD RI panel. (B) Manhattan plot for genomic association within Chr16 with all 120 strains included. (C) Manhattan plot for genomic association within Chr16 after removing the AXB/BXA RI panel. (D) Representative fluorescence images of RUNX1 (grayscale), Ki67 (yellow), cTnT (magenta) and DAPI (cyan) staining. Red arrow points to a RUNX1/Ki67 double-positive cardiomyocyte. Scale bar: 100 μm. (E) Quantification of the percentage of Runx1-positive cardiomyocyte nuclei per 20× field. All images were taken in the left ventricle at P21 comparing C57BL/6J to A/J. $n=5$ for each genotype. *P*-value calculated by two-tailed, unpaired Welch's *t*-test. (F) Quantification of Ki67-positive cells in the RUNX1-positive fraction of CM nuclei (number per 20× field). (G) Timeline depicting tamoxifen and EdU injections as well as the collection time point for the Runx1$^{OE}$ cell division experiment. (H) Percentage of MNDCMs at 4 weeks of age across Runx1$^{OE}$ and Cre-positive control (Ctrl) littermates following the injection protocol shown in G. $n=4$ Ctrl and 5 Runx1$^{OE}$. *P*-value calculated by two-tailed, unpaired Student's *t*-test. (I) Quantification of EdU-positive MNDCMs as a percentage of total EdU-positive cardiomyocytes following the injection protocol shown in G. $n=4$ Ctrl and 5 Runx1$^{OE}$. *P*-value calculated by two-tailed, unpaired Student's *t*-test. (J) Quantification of total cardiomyocyte number by hemocytometer following the injection protocol shown in G. $n=6$ for each genotype. *P*-value calculated by two-tailed, unpaired Student's *t*-test. Data are mean±s.e.m. CM, cardiomyocyte.

back at the time of the EdU injections (6-10 dpi). Thus, to determine whether cardiomyocytes overexpressing *Runx1* continue to cycle long after the normal window of post-infarction activity, we also stained for Ki67, which would identify any cycling cardiomyocyte at the time of collection. We observed a more than twofold increase in cycling cardiomyocytes in Runx1$^{OE}$ mice compared with Ctrl littermates (Fig. 5H; $P=0.002$). Finally, to determine whether the cell cycle activity observed *in situ* was indicative of bona fide proliferation we again implemented our single-cell suspension methodology (Fig. 5I). In Cre-positive Ctrl mice maintained on a C57BL/6J background, completion of cell division by cardiomyocytes was rare, with such cells identified as being

EdU-positive, mononuclear and diploid. In contrast, about 2.5% of EdU-positive cardiomyocytes labeled between days 6 and 10 post-MI were able to complete division in Runx1$^{OE}$ mice (Fig. 5J). This is less than was observed during postnatal development (Fig. 4I), but indicates that *Runx1* overexpression is sufficient to induce cardiomyocyte proliferation in adult cardiomyocytes post-MI.

## DISCUSSION
We initiated the current study with the goal of determining whether mice with divergent cardiomyocyte ploidy distribution in adulthood arrive at these end states via distinct developmental pathways. In line with previously published literature (Alkass et al., 2015;
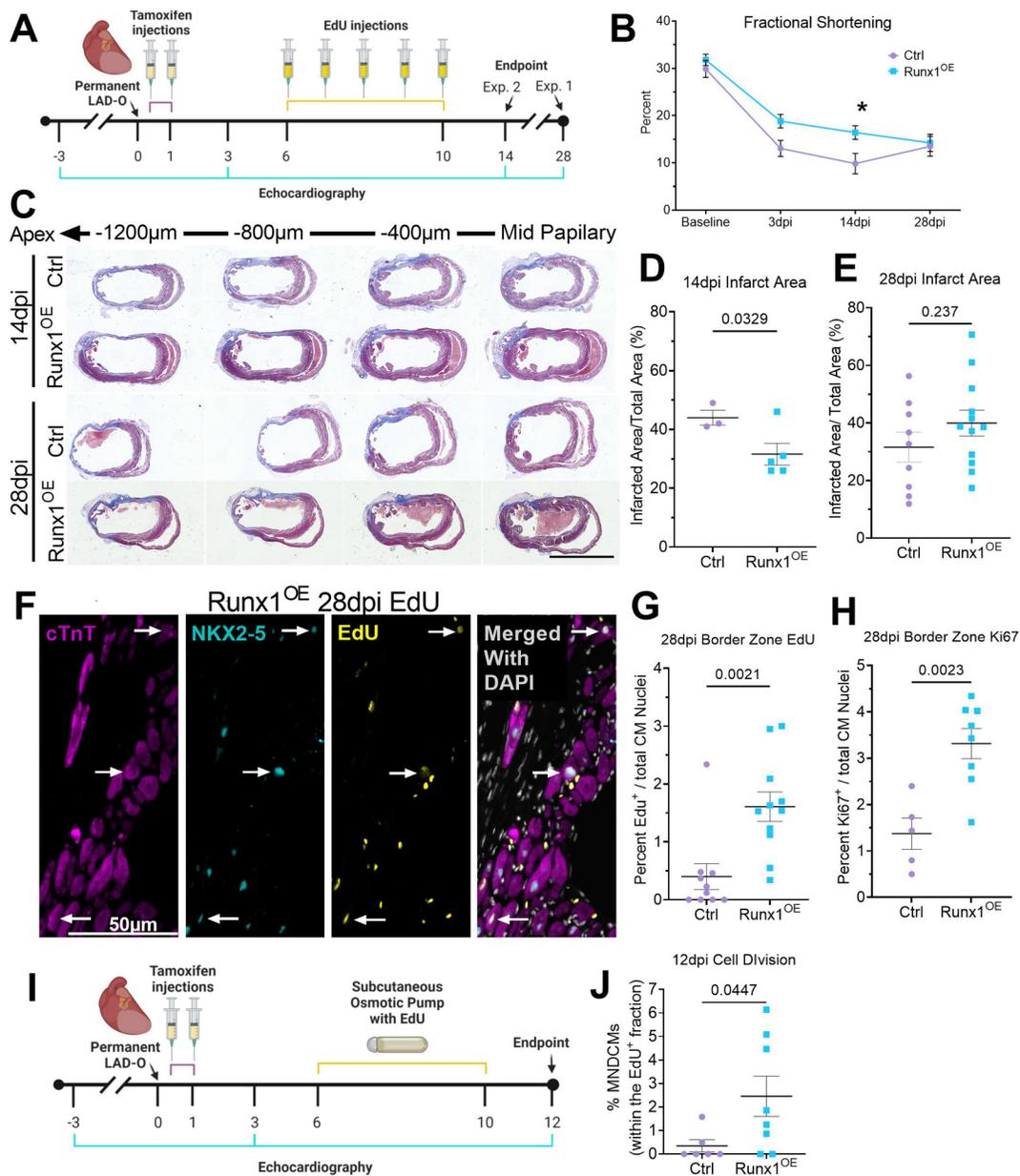
DEVELOPMENT

**Fig. 5. *Runx1* overexpression in C57BL/6J at the time of myocardial infarction transiently enhances function and induces increased cell cycle activation and completion.** (A) Experimental timelines for MI studies. (B) Fractional shortening in post-MI Ctrl and Runx1[OE] mice. *n*=10 Cre-positive controls and 13 Runx1[OE]. Statistical significance was assessed by two-way repeated measures ANOVA with Bonferroni post-hoc test. *$P$=0.0294 across genotypes at 14 dpi. (C) Representative trichrome images of Ctrl and Runx1[OE] hearts at 14 and 28 dpi. Sections were taken every 400 μm from mid papillary muscle towards the apex. Scale bar: 5 mm. (D,E) Quantification of infarcted area (blue stain in C) over total area (entire left ventricle+septum) at 14 dpi (D; *n*=3 Ctrl and 5 Runx1[OE]) and 28 dpi (E; *n*=9 Ctrl and 12 Runx1[OE]). *P*-values calculated by unpaired, two-tailed Student's *t*-test. (F) Representative immunofluorescence staining in 28 dpi Runx1[OE] cardiac tissue showing three EdU-positive CM nuclei (white arrows) in the border zone of the MI. (G) Quantification of 28 dpi border zone EdU-positive CM nuclei. *n*=10 Ctrl and 11 Runx1[OE]. *P*-values calculated by unpaired, two-tailed Student's *t*-test. (H) Quantification of 28 dpi border zone Ki67-positive CM nuclei. *n*=5 Ctrl and 8 Runx1[OE]. *P*-values calculated by unpaired, two-tailed Student's *t*-test. (I) Experimental timeline for the post-MI cell division experiment. (J) Quantification of the post-MI cell division experiment. *n*=6 Ctrl and 8 Runx1[OE]. *P*-values calculated by unpaired, two-tailed Welch's *t*-test. Data are mean±s.e.m. CM, cardiomyocyte.

Soonpaa et al., 2015), we confirmed that C57BL/6J cardiomyocytes reach their terminal composition in a linear manner. By P14, cell cycle activity in C57BL/6J cardiomyocytes is largely complete, and ploidy remains static thereafter. In contrast, A/J mice achieve their end state by a much more dynamic process. A/J cardiomyocyte polyploidy peaks around P21, after which there is a substantial expansion of the 1×2N population. Between P21 and 6 weeks of age, ploidy equilibrates, and A/J hearts arrive at their final adult

frequency of MNDCMs which is more than five times higher than that observed in C57BL/6J hearts. Concomitant with this expansion of MNDCMs in A/J, there is an increase in total cardiomyocyte numbers not observed in C57BL/6J. Using single-cell suspension methods paired with EdU labeling, we were able to identify delayed cell division events in A/J, which again were not observed in C57BL/6J. Further, there was a quantifiable decrease in polyploid cardiomyocytes, perhaps suggesting the expanding MNDCM pool

is arising from a polyploid source. This phenomenon could be akin to 'ploidy reversal', a phenomenon first reported in the liver field (Duncan et al., 2010). Mathematically, this makes sense as well – if an 8N cell is capable of reverting to a 2N state, it would generate up to four new daughter cells in the process. Therefore, our ~24,000 1×8N cells would become ~96,000 1×2N. It remains possible that other reversion combinations also ensue. For example, perhaps some of the 8N cells only revert to a 4N state – this would explain why we see such a prominent 4N population in the single-cell EdU analysis (Fig. 2F, Fig S2C,F). Regardless, the divergent processes observed when comparing two inbred mouse strains suggest that a knowledge gap remains regarding cardiomyocyte polyploidization and maturation, necessitating further experimentation on the unique phenotypic and genetic profiles across strains.

Through our examination of this MNDCM expansion unique to A/J hearts, we did not detect measurable amounts of DNA synthesis after P21, suggesting that MNDCM expansion was not achieved through canonical mitotic means (i.e. a residual MNDCM population simply proliferated through the traditional mitotic cell cycle), but rather cell cycle completion from a pre-existing polyploid cell occurred. This led us to investigate the potential for delayed cell division. A synchronous proliferative burst of cardiomyocytes from male C57BL/6J mice restricted to a narrow window of time during postnatal development has previously been reported (Naqvi et al., 2014). Although we did not observe such an expansion of cardiomyocytes in C57BL/6J, it remains possible that we missed an equivalent narrow window of cell cycle activity in A/J owing to our experimental design, which only ever tested daytime EdU incorporation.

The evaluation of cell cycle completion is limited by insufficient available experimental strategies (Auchampach et al., 2022). Traditional markers, such as aurora kinase B (AURKB), notoriously localize to the midbody in both cardiomyocytes undergoing cytokinesis and those that ultimately fail to complete cytokinesis and become multinucleated instead (Engel et al., 2006; Leone et al., 2018). Thus, on its own AURKB does not distinguish proliferation from polyploidization. Other strategies, such as the Mosaic Analysis with Double Markers (MADM) mouse (Ali et al., 2014) and sparse labeling followed by clonal analysis, have been successfully used by several groups to confirm cell division (Bradley et al., 2021; Liu et al., 2021), but require engineered alleles to be bred into the experimental model. This was not practical in our case because we hoped to compare two divergent genetic backgrounds. We instead employed a universally applicable strategy, which combines EdU labeling with Langendorff single-cell suspensions. With this method, we were able to identify cells that had definitively completed cell division in A/J hearts by 4 or 6 weeks, which were not present at P21. Furthermore, this methodology allowed powerful examination of other ploidy classes and inference of ploidy dynamics, which could not be explored by any of the histological methods described above. Admittedly, analysis of the ploidy classes by our method is largely based on ratios, and we have not excluded the potential of cell death within specific cardiomyocyte classes, which would shift these ratios. However, a general increase in the number of total cardiomyocytes after P21 indicates that this possibility is unlikely.

Our analysis of genetically divergent inbred mouse strains in a controlled laboratory setting suggests a genetic component to the regulation of polyploidization. We sought multiple strategies to identify possible mechanisms. First, a previously performed GWAS on the frequency of mononuclear cardiomyocytes (Patterson et al., 2017) provided a source of potential candidates that may reciprocally influence the unique developmental ploidy dynamics observed in A/J mice. *Tnni3k*, arising from this GWAS, has a naturally occurring polymorphism and has been previously demonstrated to control the size of the MNDCM population (Patterson et al., 2017). The variant is an alternative donor 'G' four base pairs away from the consensus exon 19-20 splice site, resulting in a frame shift and premature stop codon (Wheeler et al., 2009). Ultimately, this mutation acts as a hypomorphic allele, and is carried by A/J mice, whereas C57BL/6J carry the wild-type 'A' at this locus. Here, we show that a genetically engineered loss-of-function mutation on the C57BL/6J background partially phenocopies A/J cardiomyocyte ploidy progression. We see similar expansion of the MNDCM population between P21 and 6 weeks, as well as reduced DNA synthesis, as was recently reported (Reuter et al., 2022), and increased completion of cell division post-weaning. However, the phenotypes in the engineered *Tnni3k* null C57BL/6J mice are modest in comparison to A/J, suggesting polygenic contribution.

A second locus from the GWAS on Chr16 was *Runx1*, which has been implicated in the reversion of cardiomyocytes to a less differentiated state (D'Uva et al., 2015; Kubin et al., 2011; Zhang et al., 2016). Unlike *Tnni3k*, no obvious protein-coding mutations distinguish A/J from C57BL/6J mice within this gene. We employed epigenome-wide association analysis to identify differential methylation status within the Chr16 locus and found that the *Runx1* transcriptional start site was differentially methylated between the two strains prompting us to select *Runx1* as a candidate gene in the locus. Indeed, we found more cardiomyocytes expressing *Runx1* in A/J compared with C57BL/6J hearts at P21. Overexpression of *Runx1* in a C57BL/6J background demonstrates that *Runx1* expression alone is sufficient to increase the frequency of MNDCMs, drive cardiomyocyte proliferation, and increase total cardiomyocyte numbers in the heart. It is worth noting, however, that although we landed on *Runx1* from the Chr16 locus for a variety of reasons, there are 38 protein-coding genes within the 4.2 Mbps locus, and four other genes within the locus have protein-coding variants between A/J and C57BL/6J: *Ifnar1*, *Gart*, *Son* and *Setd4*. Of the four genes, only the variant of *Setd4* is predicted to be 'possibly damaging' by PolyPhen (Adzhubei et al., 2010) and SIFT (Ng and Henikoff, 2001), whereas the others are predicted to be benign. It remains possible that *Setd4* is a gene worth exploring in this context.

With the identification of multiple genes influencing cardiomyocyte ploidy, a subsequent question would be to ask whether the genes have combinatorial effects, i.e. epistatic, additive or synergistic. A/J mice have both a hypomorphic allele for *Tnni3k* and increased numbers of Runx1-positive cardiomyocytes. Considering the data we present here for each gene individually, it would be interesting to explore whether the two genes could have additive effects when combined, such that C57BL/6J mice with both engineered alleles begin to display A/J phenotypic levels.

The striking ploidy and proliferation phenotypes we observed during postnatal development with *Runx1* overexpression prompted us to investigate whether *Runx1* could similarly induce adult cardiomyocytes to re-enter the cell cycle and proliferate after MI. Our injury study confirms that induction of *Runx1* in cardiomyocytes at the time of injury is sufficient to induce cardiomyocyte cell cycle activation in the infarct border zone and promote proliferation. This was accompanied by a transient reduction in scar size and transient enhancement in fractional shortening compared with Ctrl mice. Recent literature, utilizing a conditional knockout allele of *Runx1*, concluded that *Runx1*

expression in cardiomyocytes led to adverse remodeling, eccentric hypertrophy and impaired calcium handling (McCarroll et al., 2018). We did not observe such adverse phenotypes by echocardiography in our shorter study; however, the benefits we did observe were notably transient in nature and our overexpression model may artificially magnify the effect of *Runx1* on cardiomyocyte proliferation. Thus, the two models address distinct biological questions that are not necessarily incompatible. Regardless, our data indicate that *Runx1* can stimulate cardiomyocyte cell cycle activation and completion in a variety of contexts.

The function of polyploidization in cardiomyocytes remains unclear. Some have suggested that developmental polyploidization, through the increase in total cellular DNA, supports enhanced rates of biosynthesis for production of contractile apparatus (Pandit et al., 2013). Others hypothesize that it promotes cell cycle exit as a strategy for both energy preservation and for preventing the disassembly of the pseudosyncitium inherent to cell division (Pandit et al., 2013). In disease contexts, many in the field postulate that MNDCMs are uniquely capable of mounting a regenerative response based on the observation that polyploidization coincides with loss of regenerative competence (Patterson and Swift, 2019). This hypothesis is supported by several recent studies where ploidy phenotypes were manipulated or altered and regeneration in turn was impacted (Gonzalez-Rosa et al., 2018; Han et al., 2020; Hirose et al., 2019; Patterson et al., 2017). Additionally, high levels of polyploidy have been observed in various cardiomyopathies and heart failure (Beltrami et al., 1997; Brodsky et al., 1994; Gilsbach et al., 2018). Despite these numerous studies, further work is warranted to determine what effect either blocking or driving the polyploidization process has on heart function. Understanding the genetic mechanisms that regulate polyploidization may improve our understanding of its role in normal cardiac physiology, myocardial regeneration and heart failure.

## MATERIALS AND METHODS
### Mice
All animal experiments were approved by and performed in accordance with the Institutional Animal Care and Use Committee of the Medical College of Wisconsin. A/J (JAX stock #000646) and C57BL/6J (JAX stock #000664) mice were either purchased from The Jackson Laboratory and allowed to acclimate for at least 1 week prior to the start of the experiment or were bred in-house from breeders originally purchased from The Jackson Laboratory. *Tnni3k* global knockout mice were generated as described by Patterson et al. (2017), G*t(Rosa)26*tm1(RUNX1)Mα mice (Qi et al., 2017; Yzaguirre et al., 2018)

were obtained from the Speck Laboratory at University of Pennsylvania, and *Myh6-MerCreMer* (JAX Stock 011038) mice were obtained from The Jackson Laboratory. All three alleles have been backcrossed and maintained for at least eight generations on a C57BL/6J background by our laboratory. For all timed experiments, birth (P0) was assumed to have taken place at 12:00 AM. Only litters with three to ten pups were used, and runts were excluded from any analysis. All experiments included a mix of virgin males and females, although sex was not determined for neonates <P21. In experiments in which a mix of the sexes was used, no phenotypic differences between the sexes were observed. Most experiments also utilized pups from multiple litters to avoid skewing of results due to a single aberrant litter. A complete list of the number of litters used and the size of the litters contributing to each experiment can be found in Table S3. Animals were housed as compatible pairs or groups in ventilated cages on 12-h light/dark cycles with *ad libitum* access to water and food. Euthanasia was performed in accordance with the recommendations of the American Veterinary Medical Association. Neonates ≤P14 were decapitated with surgical scissors, whereas animals ≥P21 underwent cervical dislocation following isoflurane-induced anesthesia.

### Tamoxifen administration
10 mg of tamoxifen (Sigma-Aldrich, T5648) was dissolved in 100 μl of pre-warmed 100% ethanol then diluted in 1.9 ml of pre-warmed sunflower oil to a final working concentration of 5 mg/ml. For neonatal induction of the *Runx1* transgene, P0 and P1 pups were injected subcutaneously with 50 mg/kg of the tamoxifen solution (∼10 μl into a 1 g pup). For induction in adults at the time of MI, mice were injected intraperitoneally with 20 mg/kg on the day of surgery and again 1 day post-MI.

### EdU administration
EdU (Thermo Fisher Scientific, E10187) was resuspended in DMSO at 100 mg/ml to create a stock solution, which was aliquoted and stored at −20°C for no longer than 3 months. A fresh, not previously thawed aliquot of stock solution was further diluted to 1 mg/ml with sterile PBS no more than 30 min prior to administration. Mice were injected once per day by i.p. injection at 10 mg/kg. Animals were euthanized at the time indicated. For a complete list of administration methods broken down by experiment, see Table 1.

### Single-cell ventricular suspensions
Hearts were extracted from euthanized mice by cutting the aorta just below the arch arteries, along with the other major vessels. Isolated hearts were washed in ice-cold KB solution and secured by their aortas to a cannula of varying sizes (see Table 2) then tied off with a 3-0 silk suture. Atria were removed with Vannas micro spring scissors. Cannulated ventricles were then hung from a Langendorff apparatus and perfused with calcium-free Tyrodes buffer, followed by 1 mg/ml collagenase type II (Thermo Fisher Scientific, 17101015) dissolved in calcium-free Tyrodes buffer. Both solutions were

**Table 1. List of EdU injection strategies by experiment**

| Figure | Age at injection(s) | Administration method | Age at euthanasia |
|---|---|---|---|
| Fig. 1F | P4 | Single i.p. injection | P5 |
| Fig. 1F | P7 | Single i.p. injection | P8 |
| Fig. 1F | P10 | Single i.p. injection | P11 |
| Fig. 1F | P21-24 | i.p. injection, once per day | P25 |
| Fig. 1F | P25-28 | i.p. injection, once per day | P29 |
| Fig. 2D | P14-20 | i.p. injection, once per day | P21 |
| Fig. 2E,F | P14-20 | i.p. injection, once per day | P21 or 6 weeks |
| Fig. S2B,C | P4 and P5 | i.p. injection, once per day | P21 or 4 weeks |
| Fig. S2E,F | P8, P10 and P12 | i.p. injection, once per day | P21 or 4 weeks |
| Fig. 3C | P14-20 | i.p. injection, once per day | P21 |
| Fig. 3D | P14-20 | i.p. injection, once per day | P21 or 6 weeks |
| Fig. 4I | P4 and P5 | i.p. injection, once per day | 4 weeks |
| Fig. 4J | P4 and P5 | i.p. injection, once per day | 4 weeks |
| Fig. 5F,G | 6-10 DPI | i.p. injection, once per day | 28 DPI |
| Fig. 5J | 6-10 DPI | ALZET Osmotic Pump | 12 DPI |

**Table 2. Cannula size by mouse age**

| Age of mouse | Cannula size | Volume of collagenase (1 mg/ml) |
|---|---|---|
| P1 | 27 gauge | 15-20 ml |
| P4-9 | 27 or 22 gauge | 20-25 ml |
| P10-20 | 22 or 20 gauge | 25 ml |
| P21 and older | 20 or 18 gauge | 25-50 ml |

warmed to 37°C. Volume of collagenase solution, along with size of cannula, varied by age of mouse (see Table 2 for details). Following perfusion, ventricular tissue was diced with dissection scissors, triturated in ice cold KB solution using a wide bore 1 ml pipette, filtered through a 250-μm mesh, and fixed by adding equal volume of 8% ice-cold paraformaldehyde (PFA) and letting it stand at room temperature (RT) for 10 min (final concentration of PFA=4%). Filtering through the 250-μm mesh was not done when assessing cardiomyocyte number. Following fixation, cell suspensions were spun down at 300 $g$ for 2 min and resuspended in PBS.

### Quantification of total cardiomyocyte numbers
Fixed, unfiltered cells resultant from a whole heart (less atria) Langendorff digestion, were resuspended in 2 ml of PBS. While fully resuspended, a 20 μl aliquot was drawn up with a 100 μl pipette and diluted 1:5 in PBS. This was repeated three separate times for each heart. Each of the three aliquots was counted in triplicate on a hemocytometer. Cardiomyocytes were distinguished from non-cardiomyocytes by size and morphology. All counts (nine in total) were averaged together to determine the best possible estimate of total cardiomyocyte numbers. A two-way ANOVA with multiple comparisons (age and strain being the two dependent variables) and Tukey post-hoc test were run to calculate the statistical significance of any inter- and intra-strain differences.

### Immunostaining of single-cell suspensions
Fixed ventricular cell suspensions were blocked with 10% normal goat serum (Thermo Fisher Scientific, 50062Z) and 0.01% Triton X-100 for 1 h at RT. Cells were incubated with primary antibody for either mouse anti-cTnT (1:500; Abcam, ab8295) or mouse anti-Actn2 (1:500; Sigma-Aldrich, A7811) in blocking solution overnight at 4°C. Cells were then washed twice in PBS with centrifugation at 300 $g$ for 3 min in between and incubated with Alexa Fluor 488 goat anti-mouse secondary (1:500; Thermo Fisher Scientific, A11029) in PBS for 1 h at RT. During the last 10 min of secondary incubation, 4′,6-diamidino-2-phenylindole (DAPI; 1 mg/ml, 1:1000) was added to the suspensions. Cells were washed twice in diH$_2$O and spun one final time. Cells from the final pellet were resuspended with Prolong Gold (Thermo Fisher Scientific, P26930), pipetted across a slide and cover-slipped.

For the cell division by single-cell suspension experiments as described by Fig. 2A, cell suspensions were also stained with a Click-iT EdU kit Alexa Fluor 555 (Thermo Fisher Scientific, C10339) according to the manufacturer's protocol. This was performed after blocking and primary antibody incubation but prior to addition of secondary antibody. The entire pellet was pipetted across slides at a density of ~15 μl of pelleted cells per slide mixed with 20 μl of Prolong Gold (Thermo Fisher Scientific, P26930) and cover-slipped.

### Ploidy analysis
Following staining, cardiomyocyte nucleation was quantified on a Nikon Eclipse 80i fluorescent microscope with a 20× objective. Three-hundred healthy cardiomyocytes were counted for their nucleation (i.e. mono- bi- tri- or tetranucleated); cardiomyocytes with a spherical shape or frayed edges (accounting for <5% of any preparation) were excluded for being dead or dying. Additionally, fluorescent images were taken at 10× magnification with a Panda PCO camera and analyzed with NIS Elements software. For each animal, the nuclei from ~500 cells were evaluated for nuclear ploidy by calculating the sum DAPI intensity of each nucleus and normalizing it to a known 2N population, typically tri- and tetranucleated cardiomyocytes. Nuclear ploidy was calculated separately for each nucleation class and the two

independent measurements were combined to estimate the frequency of each ploidy class (i.e. 1×2N; 1×4N; 1×8N; 1×16N; 2×2N; 2×4N; 2×8N; tri – 2×2N+1×4N or 2×4N+1×8N; and tetra – 4×2N or 4×4N) represented as a percentage of total. Because all ploidy subpopulations add up to 100% and are therefore interdependent on one another, a multivariate ANOVA with Tukey HSD post-hoc test was used to compare inter- and intra-strain differences.

An estimate of total number of cardiomyocytes for each ploidy class, as in Fig. 2G, was calculated by multiplying the ploidy class percentages of each individual by the average of total cardiomyocyte number at each specific time point. Changes in cardiomyocyte numbers, as in Fig. 2H, were calculated by subtracting the estimated total of a given ploidy class at 3 weeks from the estimated total of the same ploidy class at 4 weeks. Statistical significance in Fig. 2H was assessed by multivariate ANOVA comparing 3- and 4-week time points.

### Cell division analysis by single-cell suspension
As with ploidy analysis, slides were scanned in their entirety on a Nikon Eclipse 80i fluorescent microscope with a 20× objective until at least 175 EdU-positive cardiomyocytes were counted for their nucleation. Total percentages of EdU-positive cardiomyocytes in the heart were estimated using the number of EdU-positive cardiomyocytes found on a single slide multiplied by the number of slides generated following staining and divided by the total number of cardiomyocytes quantified by hemocytometer for that same animal. While scanning, images of EdU-positive cardiomyocytes pictures were taken at 10× magnification. EdU-positive cardiomyocyte nuclei were analyzed in NIS elements for DAPI intensity and normalized to a known 2N nucleus as above. At least 25 mononucleated cardiomyocytes were analyzed for each animal. A two-way ANOVA with multiple comparisons was run to show inter- and intra-strain differences.

### Surgical procedures: permanent LAD ligation and implantation of mini osmotic pump
Eight- to ten-week-old adult mice were subjected to experimental MI. Under 2-4% isoflurane, the LAD artery was permanently ligated by the rapid method and as previously described (Gao et al., 2010; Patterson et al., 2017). Some animals were subjected to a second and third surgery to install and remove an ALZET Osmotic Pumps (ALZET, 1007D) carrying 2.5 mg of EdU. Briefly, at 6 days post-MI mice were again sedated by 2-4% isoflurane and laid in the prone position. An incision of approximately 1.5 cm was made in the interscapular region and pre-loaded osmotic pumps were placed under the cutaneous layer. Surgical staples were used for wound closure and animals were wakened under a warming lamp. At 10 days post-MI, animals were again sedated, staples and osmotic pumps were removed, and incisions were re-closed with two monofilament non-absorbable sutures. In accordance with our animal protocol and the recommendations of the American Veterinary Medical Association, all mice subjected to surgical procedures were administered 1.5 mg/kg of slow-release buprenorphine via subcutaneous injection and provided with 5 mg/kg of meloxicam, administered orally for 2 days post-operation.

### Echocardiography assessment
Parameters of heart function were evaluated by echocardiography under 3% isoflurane anesthesia on uninjured animals 3 days prior to, and 3, 14 and 28 days after, MI was induced. Images were captured with a VisualSonics Vevo 3100 high resolution ultrasound and data analyzed with Vevo3100 software package. Fractional shortening was measured from M-mode conversions of short-axis views at the mid-papillary height and ejection fraction from B-mode traces of long-axis videos ensuring both the apex and central aorta were in frame. Scans, traces and analysis were performed by a reader unaware of the animal genotype. A two-way repeated measure ANOVA with Bonferroni posthoc test was used to assess statistical significance between groups at individual time points.

### Histology
As above, hearts were dissected from euthanized mice, washed in KB solution until no longer beating, and hung on a Langendorff apparatus.

Hung hearts were first perfused retro-aortically with 5 ml of calcium-free Tyrodes to flush out any remaining blood, followed by 5 ml of ice cold 4% PFA and then further fixed in 4% PFA overnight at 4°C (~12-18 h). After washing three times in PBS, hearts were stored in 70% ethanol until further processing could take place. Briefly, hearts were dehydrated by progressive introduction of ethanol (80%, 90%, 100%) and cleared with xylene prior to being embedded in paraffin wax. Embedded tissues were sectioned from apex to outflow track (two-chamber view) on a Thermo Microm HM 355S microtome at 4 μm thickness. Tissues were collected every 200-400 μm depending on the age of the animal/size of the heart.

### Trichrome stain and analysis

Gomori's trichrome was performed according to the manufacturer's protocol (Leica, 75809-284). Slides were scanned on a Keyence BZ-X810 using a 2× objective. Five consecutive sections from the mid papillary down (towards the apex) 400 μm apart were selected for analysis. MIQuant was used as described (Nascimento et al., 2011). The right ventricle and any blood or non-cardiac tissue were cleared from the analysis area before identifying 'normal tissue' and 'LV lumen'. Imaging and analysis were performed by an investigator unaware of the animal groupings. Outputs were used to calculate area of scar represented as a percentage of the total area of the left ventricle. Two-tailed Student's $t$-tests were used to calculate statistical differences across genotypes.

### *In situ* fluorescence

Tissue sections were rehydrated by sequential introduction to ethanol solutions for 2 min each (xylene, 100%, 90%, 80%, 70%, $H_2O$) and heated at 100°C in sodium citrate buffer with 0.1% Triton-X-100 and 0.05% Tween-20, pH 6.0, for 30 min for antigen retrieval. After washing in PBS, slides were blocked with 5% normal donkey serum (Jackson ImmunoResearch, 017-000-121) and 5% bovine serum albumin (VWR, 97061-420) in PBS for 1 h at RT. Primary antibodies, goat anti-NKX2-5 (1:250; Abcam, ab106923), mouse anti-cTnT (1:500; Abcam, ab8295), rabbit anti-RUNX (1:250; Abcam, ab209838) and/or rat anti-Ki67 (1:250; Invitrogen, 14-5698-82) were diluted in blocking buffer and incubated on tissue sections at 37°C for 2 h in a humid chamber. Slides were washed in PBS and incubated with secondary antibodies Alexa Fluor donkey anti-goat 555 (Thermo Fisher Scientific, A32816), donkey anti-mouse 647 (Thermo Fisher Scientific, A31571), donkey anti-rabbit 555 (Thermo Fisher Scientific, A31572), or donkey anti-rat 488 (Abcam, ab150153), respectively, diluted in PBS for 1 h at RT. Slides were washed in PBS and EdU incorporation was labeled detected using the Click-iT EdU Alexa Fluor 488 kit (Thermo Fisher Scientific, C10339) according to the manufacturer's protocol. After washing in PBS, tissues were incubated with 0.03% Sudan Black B (SBB) dissolved in 70% ethanol for 20 min at RT followed by a PBS wash. Tissues were then incubated with DAPI at 10 μg/ml in PBS for 5 mins at RT, followed by a PBS wash. Slides were cover-slipped using Prolong Gold (Thermo Fisher Scientific, P26930) and allowed to dry in the dark. Pictures were taken with a PCO Panda camera using a 20× objective on a Nikon Eclipse 80i fluorescence microscope. Approximately six pictures were taken per animal in randomly selected regions throughout the left ventricle and the septum (equal representation of each). EdU-positive NKX2-5-positive cardiomyocyte nuclei were quantified as the percentage of total NKX2-5-positive cardiomyocyte nuclei using NIS Elements software. RUNX1- and Ki67-positive cardiomyocyte nuclei were identified by intersection with cTnT and represented as positive nuclei per region. A Student's $t$-test was run between strains at each time point or between strains at a single time point.

### GWAS

Phenotypes from 120 inbred mouse strains for the HMDP were taken from Patterson et al. (2017). Averages for each strain underwent arcsin transformation to normalize the distribution of the data. Association testing was conducted on either 120 strains less the 44 strains of the BXD panel or on the 120 strains less the 27 strains of the AXB/BXA panel. Association testing of each single nucleotide polymorphism was performed in R software package as described by Rau et al. (2015).

### EWAS

The data for this portion of the study came from the control mice of a prior HMDP studying heart failure (Rau et al., 2015). Briefly, DNA was isolated from the left ventricles of 92 strains and sequenced using reduced representational bisulfite sequencing (sequencing data are available on Sequence Read Archive with the Project ID PRJNA947937). DNA methylation was called using BSSeeker2 (Guo et al., 2013) using the mm10 genome build. Hypervariable CpGs were identified as CpGs that showed greater than 25% methylation variability in at least 10% of the studied strains as previously described (Orozco et al., 2015). Phenotypes were taken from Patterson et al. (2017) as described above. EWAS was performed using the MACAU algorithm (Lea et al., 2015). Locus-wide significance was determined using the Benjamini–Hochberg correction. Locus boundaries were determined as previously described (Orozco et al., 2015).

### Data availability

Raw bisulfite sequencing used to perform the EWAS analysis have been uploaded to the Sequence Read Archive and can be found under Project ID PRJNA947937.

### People behind the papers

This article has an associated People behind the papers interview with some of the authors.

### Peer review history

The peer review history is available online at https://journals.biologists.com/dev/lookup/doi/10.1242/dev.201318.reviewer-comments.pdf

### References

**Adzhubei, I. A., Schmidt, S., Peshkin, L., Ramensky, V. E., Gerasimova, A., Bork, P., Kondrashov, A. S. and Sunyaev, S. R.** (2010). A method and server for predicting damaging missense mutations. *Nat. Methods* **7**, 248-249. doi:10.1038/nmeth0410-248

**Ali, S. R., Hippenmeyer, S., Saadat, L. V., Luo, L., Weissman, I. L. and Ardehali, R.** (2014). Existing cardiomyocytes generate cardiomyocytes at a low rate after birth in mice. *Proc. Natl. Acad. Sci. USA* **111**, 8850-8855. doi:10.1073/pnas.1408233111

**Alkass, K., Panula, J., Westman, M., Wu, T. D., Guerquin-Kern, J. L. and Bergmann, O.** (2015). No evidence for cardiomyocyte number expansion in preadolescent mice. *Cell* **163**, 1026-1036. doi:10.1016/j.cell.2015.10.035

**Auchampach, J., Han, L., Huang, G. N., Kuhn, B., Lough, J. W., O'Meara, C. C., Payumo, A. Y., Rosenthal, N. A., Sucov, H. M., Yutzey, K. E. et al.** (2022). Measuring cardiomyocyte cell-cycle activity and proliferation in the age of heart regeneration. *Am. J. Physiol. Heart Circ. Physiol.* **322**, H579-H596. doi:10.1152/ajpheart.00666.2021

**Beltrami, C. A., Di Loreto, C., Finato, N. and Yan, S. M.** (1997). DNA content in end-stage heart failure. *Adv. Clin. Pathol.* **1**, 59-73.

**Bradley, L. A., Young, A., Li, H., Billcheck, H. O. and Wolf, M. J.** (2021). Loss of endogenously cycling adult cardiomyocytes worsens myocardial function. *Circ. Res.* **128**, 155-168. doi:10.1161/CIRCRESAHA.120.318277

**Brodsky, V., Sarkisov, D. S., Arefyeva, A. M., Panova, N. W. and Gvasava, I. G.** (1994). Polyploidy in cardiac myocytes of normal and hypertrophic human hearts; range of values. *Virchows Arch.* **424**, 429-435. doi:10.1007/BF00190566

**D'Uva, G., Aharonov, A., Lauriola, M., Kain, D., Yahalom-Ronen, Y., Carvalho, S., Weisinger, K., Bassat, E., Rajchman, D., Yifa, O. et al.** (2015).

ERBB2 triggers mammalian heart regeneration by promoting cardiomyocyte dedifferentiation and proliferation. *Nat. Cell Biol.* **17**, 627-638. doi:10.1038/ncb3149

Duncan, A. W. (2013). Aneuploidy, polyploidy and ploidy reversal in the liver. *Semin. Cell Dev. Biol.* **24**, 347-356. doi:10.1016/j.semcdb.2013.01.003

Duncan, A. W., Taylor, M. H., Hickey, R. D., Hanlon Newell, A. E., Lenzi, M. L., Olson, S. B., Finegold, M. J. and Grompe, M. (2010). The ploidy conveyor of mature hepatocytes as a source of genetic variation. *Nature* **467**, 707-710. doi:10.1038/nature09414

Engel, F. B., Schebesta, M. and Keating, M. T. (2006). Anillin localization defect in cardiomyocyte binucleation. *J. Mol. Cell. Cardiol.* **41**, 601-612. doi:10.1016/j.yjmcc.2006.06.012

Gan, P., Baicu, C., Watanabe, H., Wang, K., Tao, G., Judge, D. P., Zile, M. R., Makita, T., Mukherjee, R. and Sucov, H. M. (2021). The prevalent I686T human variant and loss-of-function mutations in the cardiomyocyte-specific kinase gene TNNI3K cause adverse contractility and concentric remodeling in mice. *Hum. Mol. Genet.* **29**, 3504-3515. doi:10.1093/hmg/ddaa234

Gan, P., Patterson, M. and Sucov, H. M. (2020). Cardiomyocyte Polyploidy and Implications for Heart Regeneration. *Annu. Rev. Physiol.* **82**, 45-61. doi:10.1146/annurev-physiol-021119-034618

Gan, P., Patterson, M., Velasquez, A., Wang, K., Tian, D., Windle, J. J., Tao, G., Judge, D. P., Makita, T., Park, T. J. et al. (2019). Tnni3k alleles influence ventricular mononuclear diploid cardiomyocyte frequency. *PLoS Genet.* **15**, e1008354. doi:10.1371/journal.pgen.1008354

Gao, E., Lei, Y. H., Shang, X., Huang, Z. M., Zuo, L., Boucher, M., Fan, Q., Chuprun, J. K., Ma, X. L. and Koch, W. J. (2010). A novel and efficient model of coronary artery ligation and myocardial infarction in the mouse. *Circ. Res.* **107**, 1445-1453. doi:10.1161/CIRCRESAHA.110.223925

Gilsbach, R., Schwaderer, M., Preissl, S., Gruning, B. A., Kranzhofer, D., Schneider, P., Nuhrenberg, T. G., Mulero-Navarro, S., Weichenhan, D., Braun, C. et al. (2018). Distinct epigenetic programs regulate cardiac myocyte development and disease in the human heart in vivo. *Nat. Commun.* **9**, 391. doi:10.1038/s41467-017-02762-z

Gonzalez-Rosa, J. M., Sharpe, M., Field, D., Soonpaa, M. H., Field, L. J., Burns, C. E. and Burns, C. G. (2018). Myocardial polyploidization creates a barrier to heart regeneration in zebrafish. *Dev. Cell* **44**, 433-446.e437.

Guo, W., Fiziev, P., Yan, W., Cokus, S., Sun, X., Zhang, M. Q., Chen, P. Y. and Pellegrini, M. (2013). BS-Seeker2: a versatile aligning pipeline for bisulfite sequencing data. *BMC Genomics* **14**, 774. doi:10.1186/1471-2164-14-774

Han, L., Choudhury, S., Mich-Basso, J. D., Ammanamanchi, N., Ganapathy, B., Suresh, S., Khaladkar, M., Singh, J., Maehr, R., Zuppo, D. A. et al. (2020). Lamin B2 levels regulate polyploidization of cardiomyocyte nuclei and myocardial regeneration. *Dev. Cell* **53**, 42-59.e11. doi:10.1016/j.devcel.2020.01.030

Hirose, K., Payumo, A. Y., Cutie, S., Hoang, A., Zhang, H., Guyot, R., Lunn, D., Bigley, R. B., Yu, H., Wang, J. et al. (2019). Evidence for hormonal control of heart regenerative capacity during endothermy acquisition. *Science* **364**, 184-188. doi:10.1126/science.aar2038

Kubin, T., Poling, J., Kostin, S., Gajawada, P., Hein, S., Rees, W., Wietelmann, A., Tanaka, M., Lorchner, H., Schimanski, S. et al. (2011). Oncostatin M is a major mediator of cardiomyocyte dedifferentiation and remodeling. *Cell Stem Cell* **9**, 420-432. doi:10.1016/j.stem.2011.08.013

Lea, A. J., Tung, J. and Zhou, X. (2015). A flexible, efficient binomial mixed model for identifying differential DNA methylation in bisulfite sequencing data. *PLoS Genet.* **11**, e1005650. doi:10.1371/journal.pgen.1005650

Leone, M., Musa, G. and Engel, F. B. (2018). Cardiomyocyte binucleation is associated with aberrant mitotic microtubule distribution, mislocalization of RhoA and IQGAP3, as well as defective actomyosin ring anchorage and cleavage furrow ingression. *Cardiovasc. Res*. **114**, 1115-1131. doi:10.1093/cvr/cvy056

Liu, X., Pu, W., He, L., Li, Y., Zhao, H., Li, Y., Liu, K., Huang, X., Weng, W., Wang, Q. D. et al. (2021). Cell proliferation fate mapping reveals regional cardiomyocyte cell-cycle activity in subendocardial muscle of left ventricle. *Nat. Commun.* **12**, 5784. doi:10.1038/s41467-021-25933-5

McCarroll, C. S., He, W., Foote, K., Bradley, A., McGlynn, K., Vidler, F., Nixon, C., Nather, K., Fattah, C., Riddell, A. et al. (2018). Runx1 deficiency protects against adverse cardiac remodeling after myocardial infarction. *Circulation* **137**, 57-70. doi:10.1161/CIRCULATIONAHA.117.028911

Mollova, M., Bersell, K., Walsh, S., Savla, J., Das, L. T., Park, S. Y., Silberstein, L. E., Dos Remedios, C. G., Graham, D., Colan, S. et al. (2013). Cardiomyocyte proliferation contributes to heart growth in young humans. *Proc. Natl. Acad. Sci. USA* **110**, 1446-1451. doi:10.1073/pnas.1214608110

Naqvi, N., Li, M., Calvert, J. W., Tejada, T., Lambert, J. P., Wu, J., Kesteven, S. H., Holman, S. R., Matsuda, T., Lovelock, J. D. et al. (2014). A proliferative burst during preadolescence establishes the final cardiomyocyte number. *Cell* **157**, 795-807. doi:10.1016/j.cell.2014.03.035

Nascimento, D. S., Valente, M., Esteves, T., de Pina Mde, F., Guedes, J. G., Freire, A., Quelhas, P. and Pinto-do, O. P. (2011). MIQuant–semi-automation of infarct size assessment in models of cardiac ischemic injury. *PLoS One* **6**, e25045. doi:10.1371/journal.pone.0025045

Ng, P. C. and Henikoff, S. (2001). Predicting deleterious amino acid substitutions. *Genome Res.* **11**, 863-874. doi:10.1101/gr.176601

Orozco, L. D., Morselli, M., Rubbi, L., Guo, W., Go, J., Shi, H., Lopez, D., Furlotte, N. A., Bennett, B. J., Farber, C. R. et al. (2015). Epigenome-wide association of liver methylation patterns and complex metabolic traits in mice. *Cell Metab.* **21**, 905-917. doi:10.1016/j.cmet.2015.04.025

Orr-Weaver, T. L. (2015). When bigger is better: the role of polyploidy in organogenesis. *Trends Genet.* **31**, 307-315. doi:10.1016/j.tig.2015.03.011

Pandit, S. K., Westendorp, B. and de Bruin, A. (2013). Physiological significance of polyploidization in mammalian cells. *Trends Cell Biol.* **23**, 556-566. doi:10.1016/j.tcb.2013.06.002

Patterson, M. and Swift, S. K. (2019). Residual Diploidy in Polyploid tissues: a cellular state with enhanced proliferative capacity for tissue regeneration? *Stem Cells Dev.* **28**, 1527-1539. doi:10.1089/scd.2019.0193

Patterson, M., Barske, L., Van Handel, B., Rau, C. D., Gan, P., Sharma, A., Parikh, S., Denholtz, M., Huang, Y., Yamaguchi, Y. et al. (2017). Frequency of mononuclear diploid cardiomyocytes underlies natural variation in heart regeneration. *Nat. Genet.* **49**, 1346-1353. doi:10.1038/ng.3929

Porrello, E. R., Mahmoud, A. I., Simpson, E., Hill, J. A., Richardson, J. A., Olson, E. N. and Sadek, H. A. (2011). Transient regenerative potential of the neonatal mouse heart. *Science* **331**, 1078-1080. doi:10.1126/science.1200708

Qi, L., Huang, C., Wu, X., Tao, Y., Yan, J., Shi, T., Cao, C., Han, L., Qiu, M., Ma, Q. et al. (2017). Hierarchical specification of pruriceptors by runt-domain transcription factor Runx1. *J. Neurosci.* **37**, 5549-5561. doi:10.1523/JNEUROSCI.0094-17.2017

Rau, C. D., Parks, B., Wang, Y., Eskin, E., Simecek, P., Churchill, G. A. and Lusis, A. J. (2015). High-density genotypes of inbred mouse strains: improved power and precision of association mapping. *G3 (Bethesda)* **5**, 2021-2026. doi:10.1534/g3.115.020784

Reuter, S. P., Soonpaa, M. H., Field, D., Simpson, E., Rubart-von der Lohe, M., Lee, H. K., Sridhar, A., Ware, S. M., Green, N., Li, X. et al. (2022). Cardiac Troponin I-interacting kinase impacts cardiomyocyte s-phase activity but not cardiomyocyte proliferation. *Circulation* **147**, 142-153. doi:10.1161/CIRCULATIONAHA.122.061130

Soonpaa, M. H., Kim, K. K., Pajak, L., Franklin, M. and Field, L. J. (1996). Cardiomyocyte DNA synthesis and binucleation during murine development. *Am. J. Physiol.* **271**, H2183-H2189.

Soonpaa, M. H., Zebrowski, D. C., Platt, C., Rosenzweig, A., Engel, F. B. and Field, L. J. (2015). Cardiomyocyte Cell-Cycle Activity during Preadolescence. *Cell* **163**, 781-782. doi:10.1016/j.cell.2015.10.037

Velayutham, N., Alfieri, C. M., Agnew, E. J., Riggs, K. W., Baker, R. S., Ponny, S. R., Zafar, F. and Yutzey, K. E. (2020). Cardiomyocyte cell cycling, maturation, and growth by multinucleation in postnatal swine. *J. Mol. Cell. Cardiol.* **146**, 95-108. doi:10.1016/j.yjmcc.2020.07.004

Walsh, S., Ponten, A., Fleischmann, B. K. and Jovinge, S. (2010). Cardiomyocyte cell cycle control and growth estimation in vivo–an analysis based on cardiomyocyte nuclei. *Cardiovasc. Res.* **86**, 365-373. doi:10.1093/cvr/cvq005

Wang, J. J., Rau, C., Avetisyan, R., Ren, S., Romay, M. C., Stolin, G., Gong, K. W., Wang, Y. and Lusis, A. J. (2016). Genetic Dissection of Cardiac Remodeling in an Isoproterenol-Induced Heart Failure Mouse Model. *PLoS Genet.* **12**, e1006038. doi:10.1371/journal.pgen.1006038

Wheeler, F. C., Tang, H., Marks, O. A., Hadnott, T. N., Chu, P. L., Mao, L., Rockman, H. A. and Marchuk, D. A. (2009). Tnni3k modifies disease progression in murine models of cardiomyopathy. *PLoS Genet.* **5**, e1000647. doi:10.1371/journal.pgen.1000647

Yzaguirre, A. D., Howell, E. D., Li, Y., Liu, Z. and Speck, N. A. (2018). Runx1 is sufficient for blood cell formation from non-hemogenic endothelial cells in vivo only during early embryogenesis. *Development* **145**, dev158162. doi:10.1242/dev.158162

Zhang, X., Ma, S., Zhang, R., Li, S., Zhu, D., Han, D., Li, X., Li, C., Yan, W., Sun, D. et al. (2016). Oncostatin M-induced cardiomyocyte dedifferentiation regulates the progression of diabetic cardiomyopathy through B-Raf/Mek/Erk signaling pathway. *Acta Biochim Biophys Sin (Shanghai)* **48**, 257-265. doi:10.1093/abbs/gmv137

DEVELOPMENT